RESEARCH ARTICLE

NANO · MICRO small
www.small-journal.com

Glycerol Modulated Collagen Fibril Evolution and Lamellar Organization for Biomimetic Corneal Substitutes Construction

Kai Wu, Gaowei Li, Jiaze Gao, Yuan Tian, Dan Wei, Chengheng Wu, Jie Ding, Jing Zhu, Hongrong Luo, Jing Sun,* Seeram Ramakrishna, and Hongsong Fan*

Collagen as the main structural component of the cornea exhibits unique and highly organized fibril lamellae, which contribute to the maintenance of corneal structure and transparency. Nevertheless, collagen assembly in vitro to create ideal artificial corneal substitutes with human cornea comparable thickness and optics is still limited. Here, glycerol as a regulator can reconcile collagen thickness, transparency, and permeability, a conflicting goal by current keratoprosthesis strategies. Structure analysis reveals that glycerol treatment induces collagen hydrogels to undergo a sequential three-step multiscale structural evolution: weakened collagen crystallization at the molecular level, followed by ordered and distanced microfibril packaging at the nanoscale, and ultimately lamellar structure as well as fibril diameter and spacing-dependent optics at a macroscopic level. Such ultrastructure is then stabilized by oxazolidine crosslinking to obtain a collagen-based artificial corneal substitute (Col-Gly-OX) with optimal integration of optical clarity, mechanical robustness, high permeability, manufacturability, easy preservation and in vitro biocompatibility. Further in vivo study demonstrates that Col-Gly-OX displays excellent tissue integration, epithelialization, and stromal remodeling in a rabbit lamellar keratectomy. Overall, this work illustrates the potential of glycerol regulator to mediate the multiscale structural organization of collagen, providing a green, simple and effective strategy for the development of bionic artificial cornea.

1. Introduction

The cornea is the transparent tissue at the eye's anterior surface, which plays an important role in regulating refractive function and avoiding foreign invaders. A range of cornea-related diseases may lead to reduced vision, and in severe cases, loss of vision disease.[1] For treatment, corneal transplantation is the most effective clinical method for visual rehabilitation.[2] However, a severe global shortage of donors limits corneal transplantation.[3] Therefore, the development of simple-to-manufacture and high-performance artificial corneal substitutes is necessary to mitigate the scarcity of corneal donors.[4,5] Anatomically, collagen fibrils in the transparent corneal stroma present a lamellar structure with small and uniform diameters of ≈22.5 to 35 nm.[6] These small fibrils in each lamella are precisely organized with a high degree of lateral order and spaced apart by proteoglycans ground substance.[7,8] At the ultra-microscale, fibril is formed by the aggregation of microfibrils ≈4 nm in diameter, ordering at the telopeptide regions with crystalline packing.[9] This specific structure and arrangement of collagen from the nanoscopic to the macroscopic level endow the cornea with precise curvature and superior optics.[10,11] Therefore, the two characteristics of corneal collagen: (1) fibrils with small and uniform diameter; (2) highly organized lamellar arrangement, are believed to be a major determinant of corneal transmittance.[12] Accordingly, many studies on collagen-based artificial corneal alternatives focus on the regulation of fibril size and structure. Although various methods

K. Wu, J. Gao, Y. Tian, D. Wei, C. Wu, J. Ding, H. Luo, J. Sun, H. Fan
National Engineering Research Center for Biomaterials
College of Biomedical Engineering
Sichuan University
Chengdu, Sichuan 610065, China
E-mail: hluo@scu.edu.cn; jingsun@scu.edu.cn

G. Li
Department of Neurosurgery
West China Hospital
West China School of Medicine
Sichuan University
Chengdu, China

The ORCID identification number(s) for the author(s) of this article can be found under https://doi.org/10.1002/smll.202407606

DOI: 10.1002/smll.202407606

C. Wu
Institute of Regulatory Science for Medical Devices
Sichuan University
Chengdu 610065, China

J. Zhu
Department of Ophthalmology
The Third People's Hospital of Chengdu
The Affiliated Hospital of Southwest Jiaotong University
Chengdu 610031, China

S. Ramakrishna
Department of Mechanical Engineering
College of Design and Engineering
National University of Singapore
9 Engineering Drive 1, Singapore 117575, Singapore

have been widely reported, the construction of a stromal model with biomimetic lamella, optics, and mechanics is yet to be realized.

The collagen fibril diameter as well as the center-to-center interfibrillar spacing show considerable influence on the balance of corneal biomechanical and optical properties. In vivo, higher packing density is necessary for narrow fibrils to maintain corneal strength. Proteoglycan bridges, meanwhile, are formed between adjacent collagen fibrils and implicated in maintaining interfibrillar spacing and inhibiting lateral fibrillar over fusion, thus preserving the optical properties of the cornea.[13,14] For example, non-expression of lumican during corneal development has been found to result in a loss of cornea transparency with increased fibril diameter and decreased fibril spatial organization.[15,16] In vitro, however, collagen assembly can also be performed under physiological conditions (37 °C and neutral pH), but due to the lack of specific regulation cues, fibrils tend to over-aggregate and display poor transparency and random distribution.[17] From this perspective, exploring suitable regulators to simulate the fibril growth of corneal collagen at the molecular and microfiber levels is essential for the development of collagen-based corneal alternatives with bionic optics and mechanics.

Currently, several regulators including molecules, ions and electrons have been reported to control fibril growth in an attempt to reproduce the properties of the cornea.[10,12,18] However, without exception, these reports described the formation of a transparent but very thin collagen matrix due to the lack of regulation of fibrillar spacing. For example, Majumdar et al.[10] used cyclodextrins as a chemical cue to regulate collagen assembly during vitrification. Limited by weak intermolecular interactions between collagen and cyclodextrin, this process only resulted in corneal substitutes with a transmittance of ≈80% and a maximum thickness of ≈400 µm. Another report by Lei et al.[12] took an electrical signal as a regulator to initiate the kinetic assembly of collagen, yielding uniform and small microfibril aggregation with dense packaging which constructed an optically transparent cornea substitutes. Despite the improved transparency, limited by the triggered pH gradient width, the thickness of the assembled collagen layer can still only be within 500 µm, close to the thickness of corneal center but far from corneal limbus. Nevertheless, the root cause is that either the vitrification process or the electrical assembly will result in an uncontrollable and tightly packed lamellar structure with significantly decreased interfibrillar spacing. In this case, the thickness can only be sacrificed to obtain excellent optics, since the optical transmittance for transparent fibrous slab is negatively correlated with both fiber density and slab thickness.[19,20] Additionally, the compact packaging of small fibrils directly leads to the fact that most of these methods emphasize only optical clarity, failing to achieve mechanical robustness and high permeability. These dilemmas emphasize the need for a distinct regulator to create a transparent collagen matrix with adequate thickness and resolve the ensuing transparency and permeability conflicts.

Here, we propose the hypothesis that, under the premise of lamellar organization, a reasonable combination of fibril diameter and center-to-center interfibrillar spacing allows that a thick collagen-based corneal substitute was produced, permeability, and biomechanics. As illustrated in **Scheme 1**, glycerol, a strong polar green solvent, is selected as the regulator to induce hydrogen bond disruption and reorganization of thermally assembled crude collagen fibrils.[21] Driven by strong hydrogen bonding, collagen undergoes a multiscale structural transformation to achieve bottom-up ordered assembly and spacing rearrangement: the intermolecular crystallization of collagen is weakened at the molecular level upon enhanced hydrogen bonding between glycerol and collagen, followed by the aggregation as well as glycerol-mediated spacing of collagen chains at the nanoscale, and then the formation of small, ordered, and spaced microfibrillar clusters at the micrometer scale. The overall result is that the glycerol treatment weakens collagen crystallization, rearranging its ordered and distanced microfibril packaging, ultimately achieving lamellar structure as well as fibril diameter and spacing-dependent optics at a macroscopic level.

Compared with previous works,[10,12] the glycerol-induced structural evolution proposed in this study can easily construct bionic corneal features for collagen hydrogels, such as high transmittance and lamellar structures. Remarkably, a transparent collagen matrix with a centimeter thickness can be prepared, which is expected to be widely applied to the cornea and even deep tissue transplantation of the lens and vitreous body. Meanwhile, the spacing arrangement of collagen fibril can significantly improve hydrogel permeability to prevent vascular hyperplasia. Indeed, glycerol as a plasticizer significantly optimizes the plasticity of collagen hydrogels, giving them excellent shape adaptability and convenience for customizing complex non-planar 3D geometries.

Finally, this recombinant fibrillar structure is cross-linked and fixed to produce a stable and mechanically enhanced collagen matrix to accommodate the performance needs of the corneal prosthesis. We chose oxazolidine, a bifunctional oxazoheterocyclic derivative, as the small molecule cross-linking agent. The aim is to obtain mechanical flexibility rather than the brittle and easy-to-fracture defects associated with traditional glutaraldehyde cross-linking. The easy access and biocompatibility of collagen matrix after crosslinking are also demonstrated. Moreover, the excellent tissue integration, epithelialization, and stromal remodeling capabilities of this corneal substitute are verified by establishing a rabbit lamellar keratectomy. Overall, the collagen matrix here fulfills the bionic structure, optical clarity, and mechanical robustness necessary for an ideal corneal prosthesis, while also being highly permeable, processable, and easy to store. This simple and green approach allows for the integration of multiple high-performance metrics of the artificial cornea. Unrestricted hydrogel thickness makes this transparent collagen preparation strategy suitable not only for corneal transplantation but also for a wide range of applications in the filling of thicker transparent tissues such as the lens.

2. Results and Discussion

2.1. Glycerol Treatment of Thermo-assembled Opaque Collagen and Its Structural Transformation Determined Optical Transparency

The initial opaque collagen hydrogel (named "Col") was prepared by a most commonly used self-assembly method at neutral and

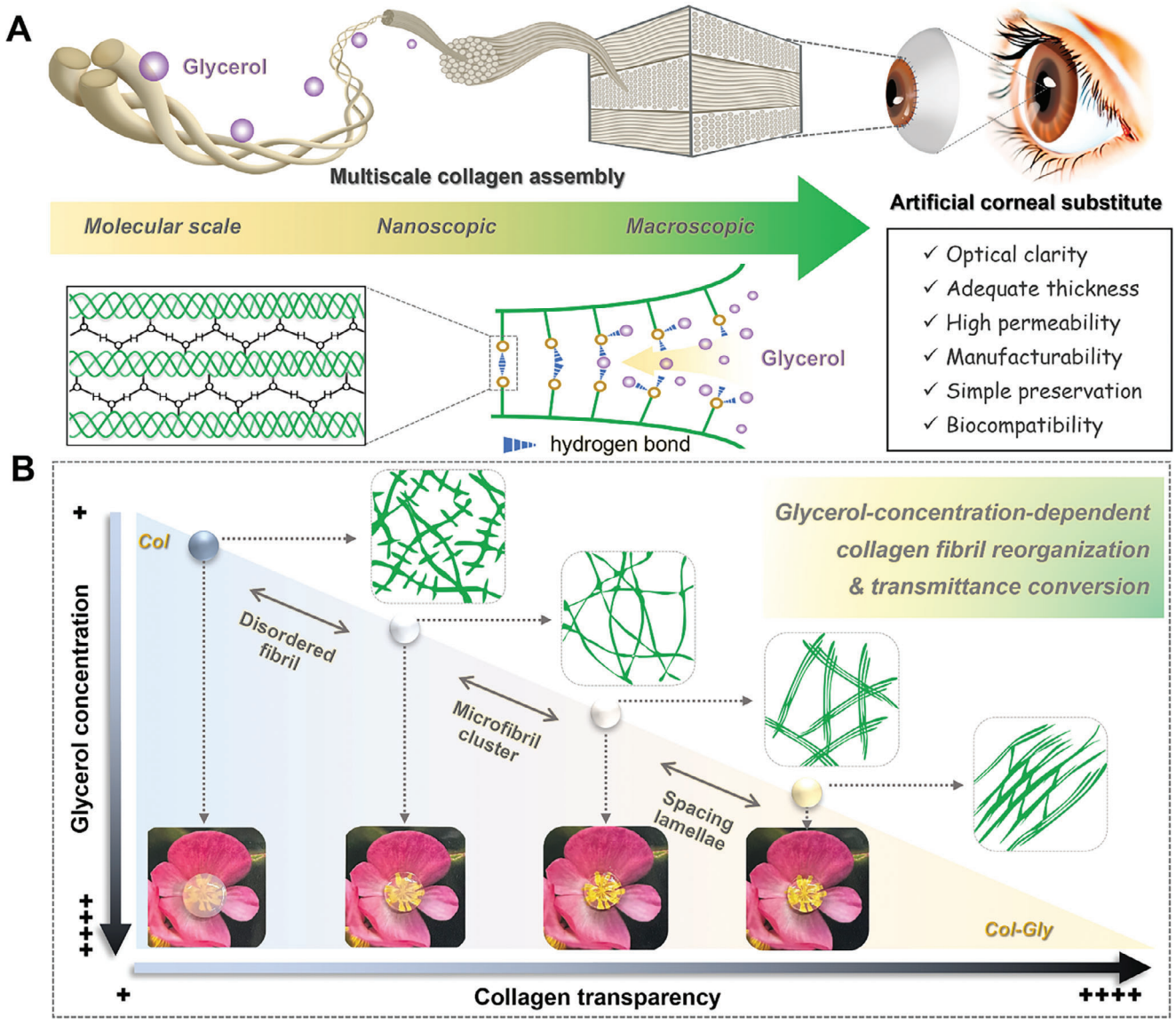

Scheme 1. Glycerol modulates the multiscale structural evolution of collagen hydrogel to create bionic artificial corneal substitutes. A) Illustration of glycerol regulating multiscale collagen assembly to achieve hydrogen bonding-driven spacing lamellae optimization. B) Glycerol-concentration-dependent fibril reorganization and the resulting transmittance conversion of collagen hydrogel.

37 °C conditions. In order to obtain hydrogels with high transparency and bionic laminar structure, we devised a simple fabrication method by soaking Col with the polar molecule glycerol (**Figure 1A**). It could be observed that the pristine opaque Col was gradually converted into a fully transparent hydrogel (named "Col-Gly") (Figure 1B). Within 20 min of glycerol treatment, Col-Gly exhibited over 95% transmittance, even superior to some of the current best-in-class keratoprostheses (Figure 1C). Particularly, the light transmittance at 550 nm obtained here was the highest compared to the representative collagen-based hydrogel matrix reported (thickness is ≈400 µm, Figure 1D).[10,12,22–24] Notably, unlike previous reports, the transparency of glycerol-induced hydrogel was almost independent of the hydrogel thickness, allowing the production of transparent 3D collagen materials up to 1 cm in thickness by a simple immersion process (Figure 1D). This progress is significant compared to other transparency strategies (only thickness below 500 µm can be achieved), and is of great interest for the transplantation and regeneration of corneal limbus and thicker transparent tissues such as lens.[10,12,18,25] In addition, glycerol treatment significantly enhanced the O_2 permeability with a value of 93.69 ± 5.9 barrers, much higher than that of conventional keratoprostheses and even close to contact lenses (Figure 1E).[26–29] We suspect that the enhanced O_2 permeability in glycerol-treated collagen hydrogels may be attributed to the fibrillar structural evolution. Microstructure analysis observed by SEM indicated that such highly transparent Col-Gly exhibited spacing distributed lamellar structure with highly ordered fibrous surface. And the ordered channels between the different fibrillar lamellas may allow the rapid passage of oxygen molecules. AFM and CLSM images further

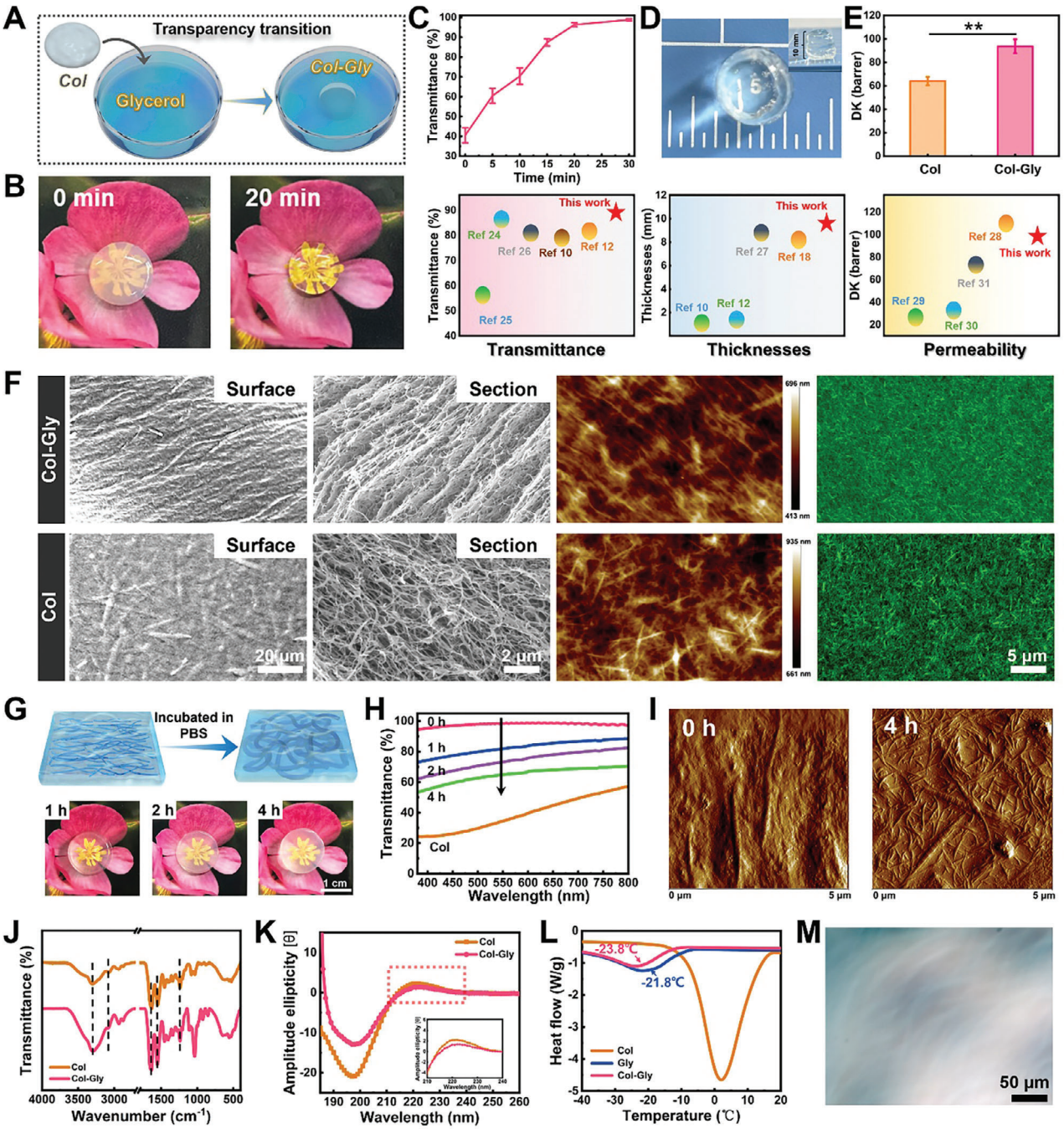

Figure 1. Glycerol initiated optical transparency, permeability and structural transformation of thermo-assembled collagen hydrogel. A) Schematic illustration of the preparation of transparent collagen hydrogel (Col-Gly) by glycerol treatment. B) The visual observation after 0 min and 20 min of glycerol treatment. C–E) Statistics and digital photograph of Col-Gly's transmittance, thickness, and oxygen permeability (top), and their comparison with other current reports (bottom). F) Fibrillar structure analysis of Col-Gly and Col observed by SEM, AFM and CLSM. G) The schematic of fibril growth and disordering in Col-Gly after PBS incubation, and the resulted optical changes after 1, 2, and 4 h of PBS incubation. H) The transmittance spectra and I) AFM images of Col-Gly after PBS treating. J) ATR-FTIR spectra. K) CD spectra. L) DSC profiles. M) Polarized optical micrograph of Col-Gly.

confirmed this microstructure organization. In contrast, a randomly distributed fibrous network with loose cross-sectional organization was observed in opaque Col (Figure 1F).

Subsequent rehydration experiments confirmed that the significant optical differences between Col-Gly and Col were closely related to their different microstructures. In brief, the as-prepared Col-Gly was incubated in PBS buffer to remove the glycerol thereby restoring the solvent composition of Col (Figure 1G). As shown in Figure 1G,H, after 4 h of PBS soaking, the transmittance of Col-Gly dropped from 95% to 60%, even approaching

to that of pure Col. AFM in Figure 1I showed that the originally small, uniform, and ordered fibrils were transformed into randomly arranged thicker fibrils. The diameters ranged from tens to hundreds of nanometers (Figure S1, Supporting Information). This phenomenon intuitively suggested that the small-sized, ordered, and lamellar fibrous structure induced by glycerol treatment is directly related to the ultra-high light transmittance of Col-Gly.

Next, we verified the effect of glycerol treatment on the molecular conformation of collagen. No new peaks appeared in the ATR-FTIR spectrum in Figure 1J, indicating the absence of chemical denaturation in Col-Gly. Moreover, the retention of characteristic amide peaks (3300, 3050, 1650, 1530, and 1250 cm^{-1}, Figure 1J) and CD peaks (a strong negative peak ≈200 nm and a positive peak ≈220 nm, Figure 1K; Figure S2, Supporting Information) also provides evidence for this. It showed the triple helix structure of collagen which indicated that collagen conformation did not influence by the glycerol. Nevertheless, CD signal attenuation of Col-Gly suggested that the addition of glycerol reduced the intramolecular interaction of collagen and disrupted fibrils' excessive aggregation. The melting temperature shift reflected by the DSC test provided evidence for this. As shown in Figure 1L, the melting temperatures of glycerol and Col-Gly are −21.8 and −23.8 °C, respectively. This decrease of melting temperature in Col-Gly precisely indicates the strong interaction between collagen and permeated glycerol molecules, which will inevitably weaken the intermolecular interaction of collagen. Further polarized light microscopy confirmed that, due to the strong hydrogen bonding of glycerol, collagen hydrogel underwent a liquid crystal transition and exhibited a nematic phase structure with a certain regular arrangement in Col-Gly, which had been proved to be related to optical transparency (Figure 1M; Figures S3 and S4, Supporting Information).[25,30]

Overall, the above phenomena indicated that glycerol treatment could rapidly transform the thermo-assembled opaque collagen hydrogel into a highly transparent one with spacing organized lamellar structure, without destroying collagen molecule conformation. Such a process can reconcile hydrogel thickness, transparency, and permeability, making these properties equal or exceed the most advanced corneal substitutes.

2.2. Structural Evolution at Multiscale during Glycerol Treatment

To shed light on the underlying mechanism by which glycerol regulating the structural reorganization of collagen fibrils, an array of analyses was further conducted to unveil hierarchical discrepancies as treatment proceeding. It was worth noting that the process of glycerol treatment was not only time-dependent but also somewhat concentration-dependent. As shown in Figure S5, Supporting Information and the inserted image in **Figure** 2A, visual inspection suggested that the light transmission of the collagen hydrogel gradually improved with the increase of glycerol concentration. High-resolution TEM was used to investigate microstructure changes with glycerol concentration. As indicated in Figure 2A, collagen fibril size as well as size distribution decreased visually with the increasing glycerol concentration, and gradually exhibited oriented clusters of microfibril aggregation. Based on this phenomenon, we proposed the hypothesis that glycerol treatment induces a multiscale structural transformation of collagen fibrils, leading to the emergence of a highly transparent appearance and spacing lamellar structure (Figure 2B–D).[31]

At the microscale level, glycerol treatment induced hydrogen bond breaking of collagen fibrils, leading to a decrease in fibril size and an increase in microfibril density (Figure 2B). We speculate that this is the underlying reason for the hyalinization of collagen. The statistics of fibril diameter and phase volume fraction provided evidence for this. As shown in Figure 2B-i, with increase of glycerol concentration (from 20% to 100%), the transmittance of the initial opaque collagen hydrogel (<45%) was transformed to 58, 64, 82, 92, and 95.5% sequentially. And the glycerol content within Col-Gly was calculated to be 20%, 35%, 49.9%, 56.8%, and 57% sequentially, with increase of glycerol concentration from 20% to 100% (Figure S6, Supporting Information). This result suggested that with the increase of glycerol concentration, the actual glycerol content within the hydrogel increased continuously, and reached equilibrium when the glycerol concentration was above 80%. It is also consistent with the little transmittance difference between 80% and 100% glycerol-treated hydrogel groups observed in Figure 2B-i. Correspondingly, the initial size of crude fibril (close to 50 nm) gradually decreased to 29, 22.5, 12, 10, and 8 nm, while the volume fraction of fiber phase increased to 20, 25, 33, 58, and 80% (Figure 2B-ii). These results, together with the rehydration test in Figure 1G above, corroborate that the transparency transition of collagen is directly related to the formation of small, tightly packed collagen microfibrils. This is consistent with literature reports,[10,12] but these studies do not rationalize the driving processes of fibril structural change. In this experiment, we emphasize that only when the concentration of glycerol reached more than 60%, a fundamental shift in hydrogel transmittance occurred, in parallel with an extremely rapid change in fibril size and phase volume. At this stage, however, the water content of hydrogel remained almost stable, although it had previously decreased sharply due to osmotic pressure-induced shrinkage of the hydrogel volume (Figure 2B-iii). This excludes the possibility that shrinkage-driven fiber densification led to a shift in collagen hyalinization. As a consequence, we conclude that the high concentration of glycerol treatment induces hydrogen bond disruption and reorganization of collagen fibrils, which in turn drives the fibril structural transformation that ultimately led to collagen transparency.

It is worth noting that even with a transmittance of up to 96% (Col treated with 100% glycerol), the fibril density of Col-Gly was only 0.08 g cm^{-3}. This value is more than ten times lower than that of other methods, for example, 0.88 g cm^{-3} obtained by the recently reported electro-assembly method.[12] The transmittance (T) can be calculated generally by the Chandrasekhar's radiative transfer Equation (1):

$$T = \frac{1}{1 + 0.75\rho\sigma_{sct}h} \quad (1)$$

where h is the thickness, ρ is the fibril density, and σ_{sct} is the scattering cross section, the magnitude of which is proportional to the cube of the fibril diameter.[19] According to the equation, the optical transmittance of nanoscaled fibrillar slab could be greatly improved by reducing the fibril diameter and density. Compared with the electro-assembled collagen, fibril diameter obtained by

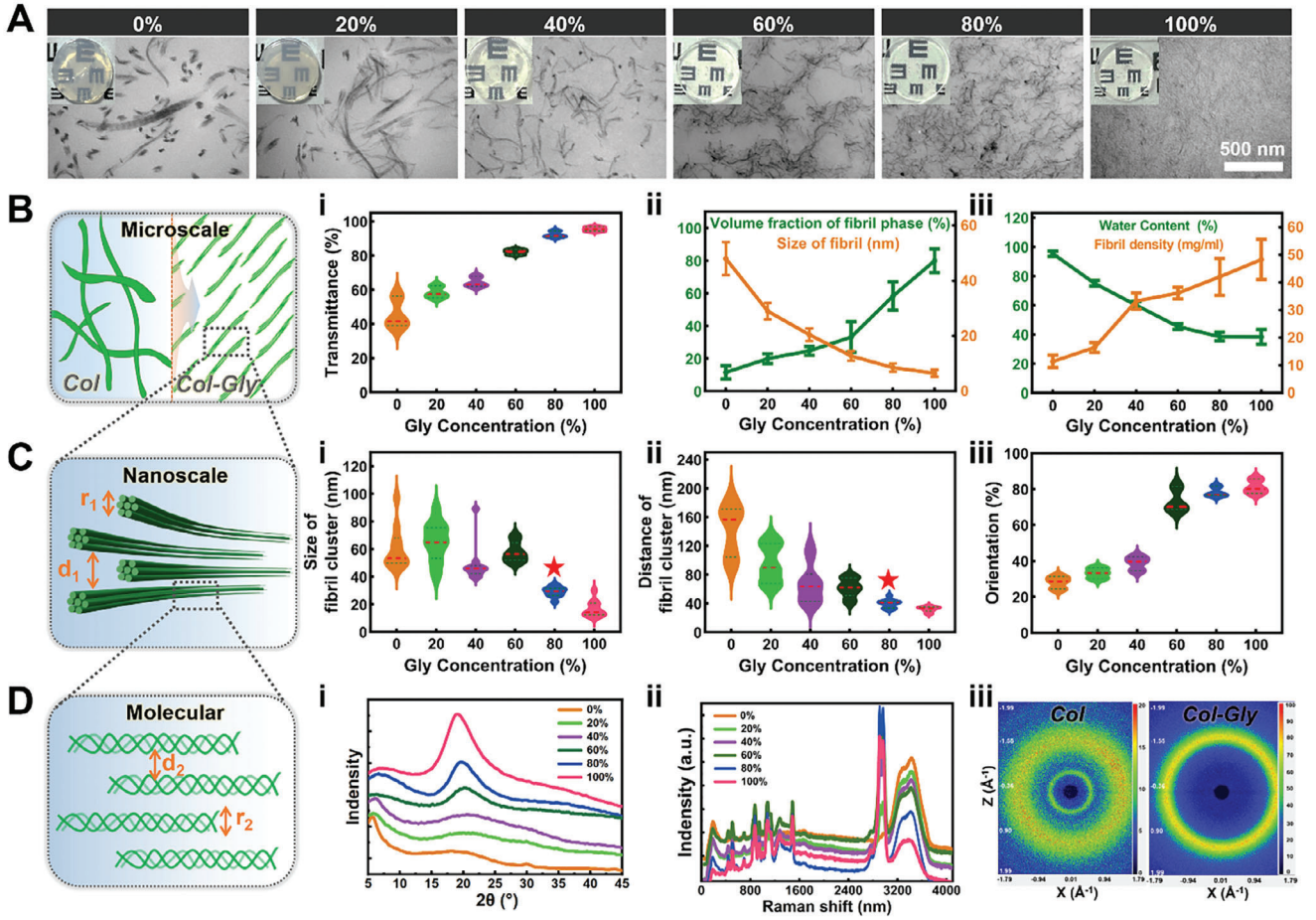

Figure 2. Multiscale structural evolution of Col-Gly during glycerol treatment. A) TEM images of Col-Gly treated with different concentrations of glycerol (0%, 20%, 40%, 60%, 80%, 100%). The inset images show visual observation of hydrogel transparency. B) Illustrations of the microscale fibril morphology of Col-Gly: B-i) transmittance, B-ii) fibril size and volume fraction of the fiber phase, B-iii) water content and collagen fibril density. C) Illustrations of the nanoscale microfibril clusters of Col-Gly: C-i) cluster size, C-ii) distance between neighboring clusters, C-iii) cluster orientation. D) Illustrations of molecular packing of Col-Gly: D-i) XRD spectra, D-ii) Raman spectra, D-iii) Debye scattering rings of 2D SAXS patterns for Col (left) and Col-Gly (right).

our method is equivalent to that reported ≈10 nm, however, the density (ρ) is ten times less. Hence, in the case of comparable transmittance (T), our hydrogel thickness (h) can be much larger. This is why our method enables the preparation of collagen hydrogels with high transmittance at centimeter-scale thickness.

Subsequently, it is confirmed that the above low density of collagen fibrils is associated with the formation and spacing arrangement of microfibril clusters on the nanoscale. TEM images in Figure 2A showed that along with glycerol treatment, cluster-like microfiber aggregations with uniform spacing distribution gradually appeared, which were clearly observed when the glycerol concentration was above 60%. This phenomenon is different from any previous reports. As shown in Figure 2C, we defined the diameter of the clusters as r_1, and the distance between neighboring clusters as d_1. Statistics showed that with the increase of glycerol concentration, both r_1 and d_1 decreased continuously (Figure 2C-i,ii). In particular, the collagen hydrogel treated with 80% concentration of glycerol had r_1 and d_1 of 29 and 40 nm, respectively, which closely matched the collagen fibril diameter and interfibrillar spacing of corneal tissue.[32,33] It has been reported that the formation of lamellar orientation required both an attractive force to aggregate collagen molecules into fibrils and a repulsive force to induce liquid crystalline order within these fibrils.[34] The balance between these forces prevented agglomeration, facilitating the creation of corneal-like lamellar matrices. Regulators of collagen fibrillar order in the cornea, such as proteoglycans and ions, can help us understand the driving forces. For example, Knupp et al. proposed that proteoglycan bridges formed between adjacent corneal collagen fibrils exert opposing forces on the collagen, with a repulsive force arising from osmotic pressure and an attractive force arising from the thermal motion of the proteoglycans.[35] Regini and Elliott showed that, with the increase of NaCl concentration, chloride ions bind more and more tightly to collagen fibrils, resulting in additional repulsion between fibrils and thereby improving fibril ordering and thus transparency.[36,37]

Herein, we reason that intermolecular hydrogen bonding of collagen induces microfibril aggregation, while the interaction between glycerol and collagen compartments the aggregations. Ultimately, clustering and spacing rearrangements of collagen microfibrils were achieved, allowing the obtaining of transparent collagen with a much lower fiber density than previously

reported methods. In addition, treatment with high concentration glycerol significantly promoted the mono-dispersity and ordered arrangement of collagen microfibrils, which is also important for high transmittance due to reduced light scattering (Figure 2C-iii; Figure S7, Supporting Information). Although the scattering has been ascribed to the collagen fibril evolution caused to the lamellar organization, theory predicts that light scattering could decrease if there is a decreased mismatch in the refractive index of the collagen fibrils and the solvent around them. The dry collagen fibrils have a refractive index of 1.55, whereas the water distributed has a refractive index of 1.33 and, on the basis of this difference, the Col should scatter a large amount of incident light.[38] After the treatment with glycerol with a refractive index of 1.47, the extra solvent in the extrafibrillar space would reduce light scatter by lowering the refractive index mis-match between the fibrils and the surrounding environment.[39,40] The actual effect of such a change is difficult to assess since the glycerol intrusion is accompanied by changes in other parameters on which transmission depends, such as fibril size and arrangement.

The molecular packing of collagen was further examined using X-ray diffraction (XRD). As shown in Figure 2D, the size of a collagen molecule is defined as r_2 and the distance between molecules is defined as d_2. The results of the previous experiments found that glycerol treatment does not alter the structure and basic size (r_2) of collagen molecules. As presented in Figure 2D-i, all collagen hydrogel samples showed two diffraction peaks at $2\theta = \approx 5–10°$ and 20°, corresponding to the crystalline domain and amorphous region, respectively.[41,42] As the glycerol concentration increased gradually, the sharp low-angle peak shifted toward higher angles and broadened, while the broad high-angle peak exhibited the opposite behavior.

According to the Bragg's equation, the average size of the distance between molecules (d_2) decreased from 1.52 nm in initial Col to 1.28 nm in the 80% glycerol-treated group (Figure S8, Supporting Information). The decreased crystallinity indicated an enhanced interaction between glycerol molecule and collagen chain, as well as a reduction in hydrogen bonding between the collagen molecular chains.[43] This result was further supported by the gradual weakening of the hydroxyl stretching vibrational peaks (3100–3600 cm^{-1}) in the Raman spectra (Figure 2D-ii). Meanwhile, as illustrated in Figure 2D-iii, the 2D SAXS patterns for Col showed a clear Debye scattering ring with a maximum intensity at $q = 1.35$ nm^{-1}, indicating the presence of higher crystallinity. By contrast, the transparent collagen hydrogel obtained by 80% glycerol treatment exhibited a reduced number of diffraction rings and fewer crystalline surfaces. The diffraction peak at $2\theta = 20°$ in Figure 2D-i and at $q = 1.4$ $Å^{-1}$ in Figure S9, Supporting Information, gradually became sharper, agreeing to indicate a more ordered lattice arrangement and fiber orientation of collagen. This was particularly intriguing since the transparency of the cornea was typically associated with the alignment of fibrils within a highly ordered lattice.

Overall, glycerol-induced hydrogen bonding reorganization and the resulting spacing lamellae as well as transmittance modulation of collagen hydrogel undergoes a sequential three-step multiscale structural evolution: (1) weakened crystallization of collagen molecules at the molecular level; (2) distancing of collagen polymer chain assembly at the nanoscale; (3) spacing arrangement of ordered microfibril clusters at a macroscopic level. Considering the bionic fibrillar structure and optical transmittance, the transparent collagen hydrogel obtained by treating with 80% concentration glycerol was selected for following experiments.

2.3. Preparation and Characterization of Oxazolidine Derivative Crosslinked Col-Gly (Col-Gly-OX) as Artificial Corneal Substitutes

We further proposed a chemical cross-linking strategy to permanently immobilize the obtained fibril structure with spacing lamella to protect Col-Gly from fibril disruption or recombining due to glycerol leakage. Besides, the crosslinking step could simultaneously solve the problem of poor mechanical properties commonly faced by current cornea scaffolds.[44] Considering that conventional glutaraldehyde (GA) crosslinker caused brittleness and yellowing of protein-based materials, we tried a bicyclic oxazolidine-based crosslinker (OX), and their crosslinking process was shown in **Figure 3**A. Figure 3B illustrated the synthetic route of OX and confirmed its successful synthesis by ^{1}H NMR spectroscopy. The mechanism of cross-linking of OX with proteins is a complex but not fully understood process, involving ring opening, addition and subsequent reaction steps.[45–47] Present studies have confirmed that OX first undergoes a ring-opening reaction to form an unstable carbon-positive intermediate under appropriate pH and temperature conditions. This intermediate is highly reactive and can undergo addition reactions with amino groups in proteins (mainly the side chain amino groups of basic amino acids such as lysine), which has been demonstrated in a latest report.[48] The cross-linking sites formed through the above steps can further react with other amino acid residues or amino groups on other protein molecules to form a more complex covalent cross-linking network and enhance the physical properties of the collagen hydrogels (Figure S10, Supporting Information).

Quantitative analysis of optics showed that Col-Gly-OX still exhibited high transparency (>90%, Figure 3C) and low haze (<20%, Figure 3D). Also, we verified whether the medium around the hydrogel may have an effect on the measurement of optical properties. Results showed that there was no significant difference between the transmittance measured under PBS immersion and air exposure, both for Col-Gly-OX and Col-Gly-GA (Figure S11, Supporting Information). Therefore, in the following long-term optical property monitoring, we do not emphasize the difference in the measurement medium. It is worth noting that Col-Gly-OX is obtained by reacting Col-Gly with OX and then washing several times. This ensures that free glycerol and unreacted crosslinkers are completely removed from Col-Gly-OX, thus avoiding changes in hydrogel structure and refractive index that might be caused by glycerol diffusion during subsequent immersion. And Col-Gly-OX maintains almost equal transmittance as Col-Gly, implying that the refractive index of glycerol itself may not be the main factor causing transparent transition of collagen. In our experiment, we put more emphasis on glycerol as a regulator that led to the evolution of small, uniform, ordered, and spaced collagen fibril, thereby reducing light scattering and consequently increasing the overall transmittance of the hydrogel. The excellent optical performance was the demonstrated to be consistently maintained over 8 weeks of immersion in artificial

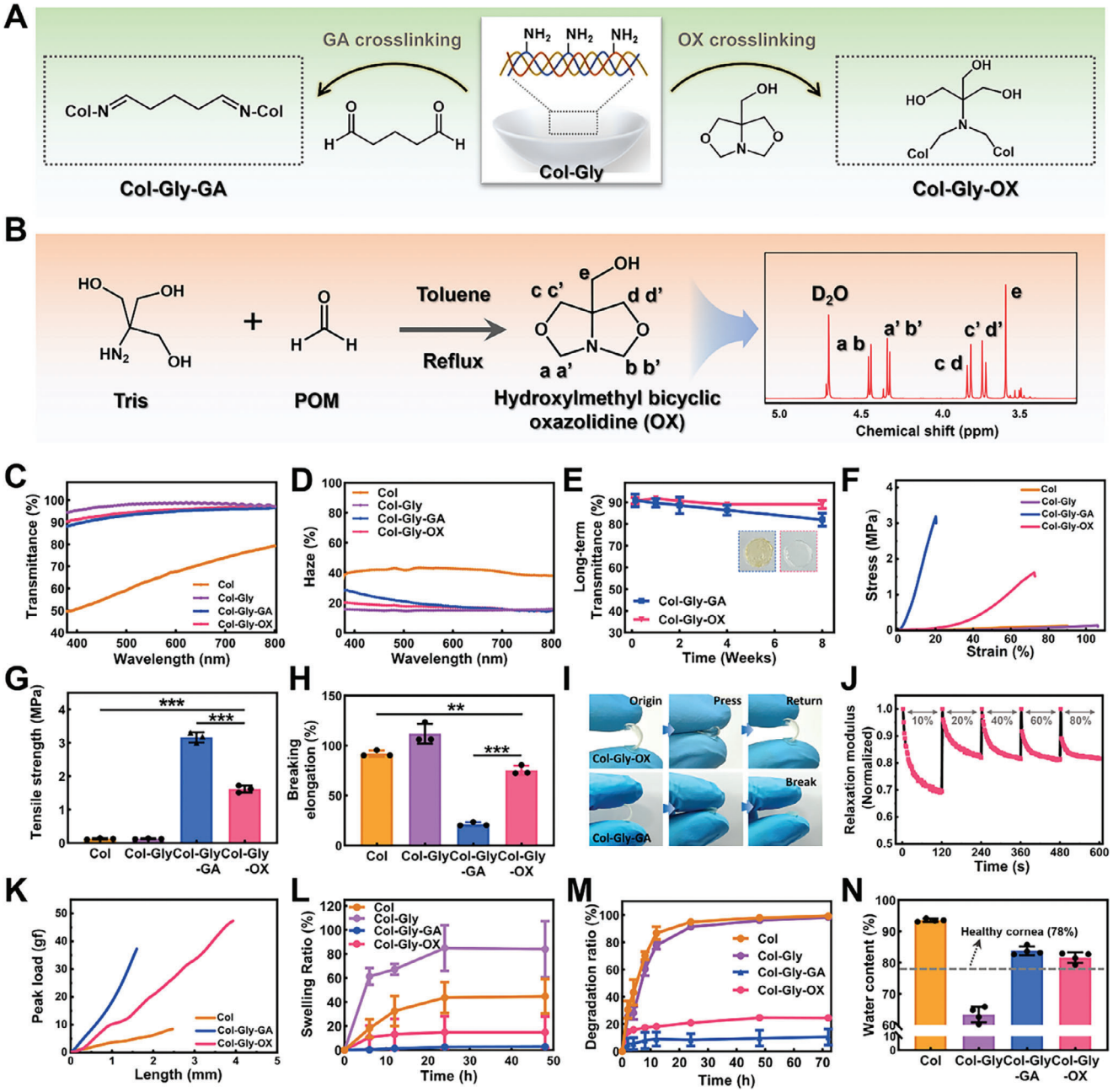

Figure 3. Physicochemical performance of Col-Gly-OX as artificial corneal substitutes. A) Schematic illustration of the oxazolidine derivative (OX)- and glutaraldehyde (GA)-crosslinking principle. B) Synthetic route and ^{1}H NMR spectrum of OX. C) The transmittance spectra and D) haze spectra of Col, Col-Gly, Col-Gly-GA and Col-Gly-OX in the visible light range. E) The long-term transmittance of Col-Gly-GA and Col-Gly-OX after immersing in sterile artificial tears. The insets represent optical pictures of Col-Gly-GA (left) and Col-Gly-OX (right) after 8 weeks of immersion. F) Typical stress-strain tests. G) Quantitative tensile strength and H) breaking elongation. I) Images of Col-Gly-OX (top) and Col-Gly-GA (bottom) hydrogel sheets after 180° folding. J) Consecutive stress relaxation of Col-Gly-OX. K) Typical suture-pullout curves. L) Swelling ratio. M) Degradation curve. N) Saturated water content.

tears, suggesting a long-term optical stability of Col-Gly-OX. In contrast, the transmittance of Col-Gly-GA (GA crosslinked Col-Gly) was similar to that of Col-Gly-OX at the initial stage of immersion, however, gradually decreased over time and yellowed in appearance after 8 weeks (Figure 3E).

Specifically, SEM images show that the Col-Gly hydrogel after OX cross-linking still has a distinct lamellar structure (Figure S12, Supporting Information). Furthermore, the mechanical properties of Col-Gly were systematically studied before and after chemical crosslinking. As depicted in Figure 3F,H, the tensile strength and breaking elongation of Col-Gly-OX showed a substantial enhancement, and reached 1.617 MPa and 75.3 ± 3%, respectively. Notably, the breaking elongation of Col-Gly-OX increased almost fourfold compared to Col-Gly-GA,

suggesting a malleability advantage in the face of ocular hypertension. In addition, the Young's modulus of Col-Gly-OX was significantly improved, reaching 1.975 MPa (Figure S13, Supporting Information). Since the elastic modulus of corneal tissues has been reported to range between 1.14 and 2.63 MPa,[49] Col-Gly-OX here exhibits a biological cornea-matching mechanics. The bending-recovering experiment intuitively demonstrated the excellent flexibility of Col-Gly-OX, which recovered without damage after folding, while Col-Gly-GA suffered a brittle fracture (Figure 3I). Furthermore, consecutive stress relaxation cycles suggested that the relaxation time was largely independent of the strain level, indicating that Co-Gly-OX had good mechanical stability (Figure 3J). Subsequent classic suture pull-out test in Figure 3K showed that the Col-Gly-OX could withstand significantly greater loads (≈50 gf) before rupture compared to Col-Gly-GA (≈37.3 gf). The suture resistance value far exceeded the interrupted suture required in clinical practice (30 gf), indicating that Col-Gly-OX could meet the mechanical requirements of implant surgery.[10]

The stability and degradation resistance of Col-Gly were also improved by OX crosslinking, which better meets the needs of in vivo applications of corneal substitutes. As shown in Figure 3L, both OX and GA crosslinking significantly improved Col-Gly's stability since less than 20% swelling occurred after 72 h of corrosion in artificial tears. Figure 3M verified the enhanced anti-enzymatic hydrolysis ability of Col-Gly-OX, and the degradation rate was only about 20% after 72 h of incubation in PBS solution containing collagenase. Notably, the light transmittance of Col-Gly-OX and Col-Gly-GA both decreased to a certain extent after degradation, but still maintained about 80% transmittance at 550 nm (Figure S14, Supporting Information), basically meeting the needs of corneal treatment.[10,50] Besides, OX crosslinking optimized the hydrophilicity of Col-Gly, reaching a water content of 81.6 ± 1.66% close to that of native cornea (≈78%) (Figure 3N; Figure S15, Supporting Information).[51] Taken together, these results reveal robust mechanical properties and structural stability of Col-Gly-OX, as well as its ultra-high light transparency. In particular, Col-Gly-OX is superior to the conventional GA crosslinked collagen hydrogels in long-term optical stability, flexibility, suture performance and other comprehensive properties, which can better meet the needs of corneal transplantation in clinical practice.

2.4. Manufacturability, Storage, and In Vitro Biocompatibility of Col-Gly-OX Artificial Corneal Substitute

Glycerol here could not only quickly improve the light transmittance of collagen hydrogels, but also enhance the plasticity of hydrogel to adapt 2D and 3D shapes. As displayed in **Figure** 4A, Col-Gly can be easily shaped into circles and pentagrams, and also, can be adapted to different surfaces to create complex 3D geometries (hemispherical, tubular, etc.). Figure 4B illustrated a schematic fabricating process of Col-Gly-OX artificial corneal substitute in a customized mold, including reshaping, demolding, and crosslinking. The digital photographs indicated that Col-Gly-OX with special curvature could be conveniently obtained to adapt to the ocular surface, presenting excellent transparency. Fascinatingly, Col-Gly-OX hydrogel could maintain a flat surface morphology after freeze-drying, resulting in a dry corneal substitute that is easy to store. After rehydration and swelling, the dry Col-Gly-OX film regained its original curvature and smooth wetted surfaces, which is beneficial to alleviate the discomfort after implantation in the eye. Moreover, false color view and 3D view images of the Col-Gly-OX film surface detected by optical 3D surface profiler showed that the overall surface of the Col-Gly-OX film was smooth with little undulations (Figure S16, Supporting Information). Whereas the dry Col-Gly-GA film showed significant rough wrinkles and had difficulty in rehydrating to smooth hydrogel (Figure S17, Supporting Information). It is well known that one of the major factors that make it difficult to popularize the use of corneal substitutes is their logistical constraints (including transportation, preservation, etc.).[52] From this perspective, Col-Gly-OX is very promising to be developed as an easy-to-store, rehydrated ready-to-use product. This will greatly promote the design of corneal substitutes with simple preservation and easy access, which is conducive to solving the problem of corneal donor use under emergency conditions.

The biocompatibility of Col-Gly-OX artificial corneal substitute was further investigated by cell proliferation and migration experiments. As shown in Figure 4C, human corneal epithelial cells (HCECs) spread and proliferated continuously on the surface of Col-Gly-OX (Figure S18, Supporting Information). After 5 days of culture, the cellular viability on the surface of Col-Gly-OX was nearly 100%, which is comparable to that of the control. In contrast, the cell viability on the surface of Col-Gly-GA was slightly lower, confirming that Col-Gly-OX had better cell proliferation ability (Figure 4D). Cell migration ability is important in epithelialization for corneal injury repair. The in vitro scratch assay shown in Figure 4E,F demonstrated that the HCECs on the surface of Col-Gly-OX could migrate to the scratched area (about 450–500 μm distance) within 36 h, significantly faster than that of Col-Gly-GA and control. The favorable cell biocompatibility as well as cell migration ability made Col-Gly-OX a promising candidate for corneal tissue engineering to repair corneal defects.

2.5. In Vivo Epithelialization and Cornea Restoration of Col-Gly-OX Artificial Corneal Substitute

To further investigate whether these hydrogels with excellent mechanics and optics could promote cornea repair, a corneal lamellar transplant model were used in vivo studies (**Figure** 5A; Figure S19, Supporting Information). Wherein the Col-Gly-OX and Col-Gly-GA implants were used as experimental groups, and only corneal defects were created without any materials on the wounded recipient bed as a control. After hydrogel implantation, the re-epithelialization progress of corneal defects was monitored by regular optical and fluorescein staining observation via slit-lamp microscopy. As shown in Figure 5B,C, defective corneas with Col-Gly-OX implantation remained transparent and underwent extremely low leveled neovascularization during 8 weeks of surgery (Figure S20, Supporting Information). Fluorescein stained slit lamp photographs showed a homogeneous and rapid epithelialization process in the Col-Gly-OX group, with almost complete healing after 4 weeks of implantation (Figure 5B,D). In contrast, some corneal haze and neovascularization were

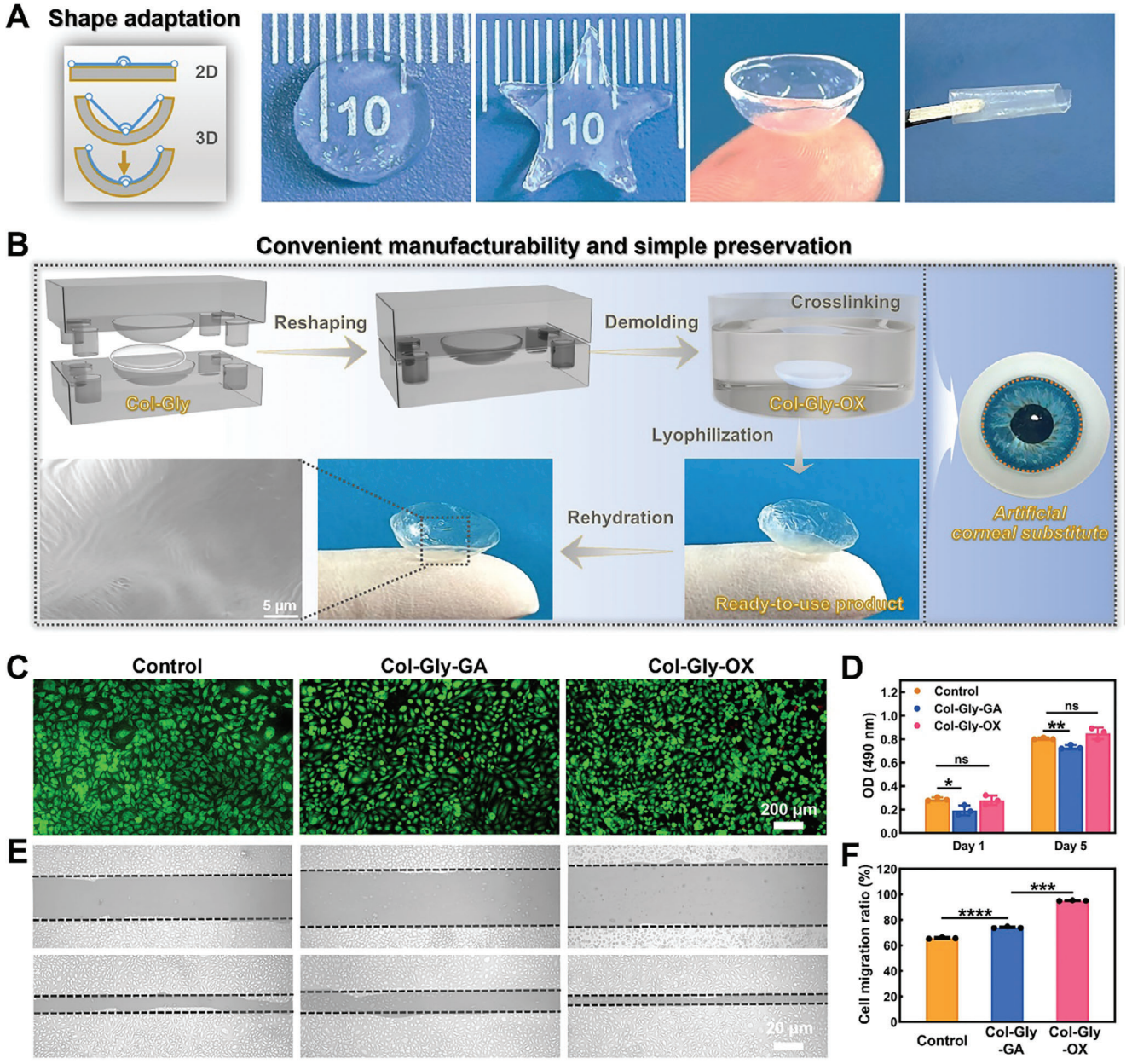

Figure 4. Shape adaptation, manufacturability, simple preservation and in vitro biocompatibility of Col-Gly-OX. A) Preparation schematic and digital photographs of Col-Gly-OX with circular, pentagonal, hemispherical and tubular shape. B) Schematic illustration of customizing Col-Gly-OX artificial corneal substitute with specific curvature. Subsequent freeze-dried and rehydrated photographs with smoothness and curvature retention indicate that Col-Gly-OX can be developed as an easy-to-store and ready-to-use product. C) Live (green) /dead (red) staining and D) cell activity statistics of HCECs cultured on the surface of Col-Gly-GA and Col-Gly-OX after 5 days (n = 3). Cells cultured on the plate was used as a control. E) Scratch assay images and F) cell migration area quantification of HCECs after 0 and 36 h incubation (n = 3). The values are mean ± SD. p-Values: *$p < 0.05$, **$p < 0.01$, ***$p < 0.001$, and ****$p < 0.0001$.

consistently observed in the Col-Gly-GA group, which probably resulted from inflammation or infection after keratoplasty.

Anterior segment optical coherence tomography (AS-OCT) was conducted to observe the cross-sectional images of the corneal tissue. Results showed that Col-Gly-OX integrated well with the corneal stroma, and the interface began to disappear 1 week postoperatively (Figure 5E). After 8 weeks, the formation of dense stromal tissue and newly formed corneal epithelium was clearly observed. By contrast, Col-Gly-GA group showed poor tissue integration and exposed a visible scarring, resulting in a distinctly shaded area in the OCT image. It should be noted that the control group also showed a transparent epithelialized layer, however, underwent more severe edema and relatively low stromal. Overall, Col-Gly-OX displays better tissue integration and less inflammatory response, which benefits subsequent rapid corneal epithelialization and thickness restoration.

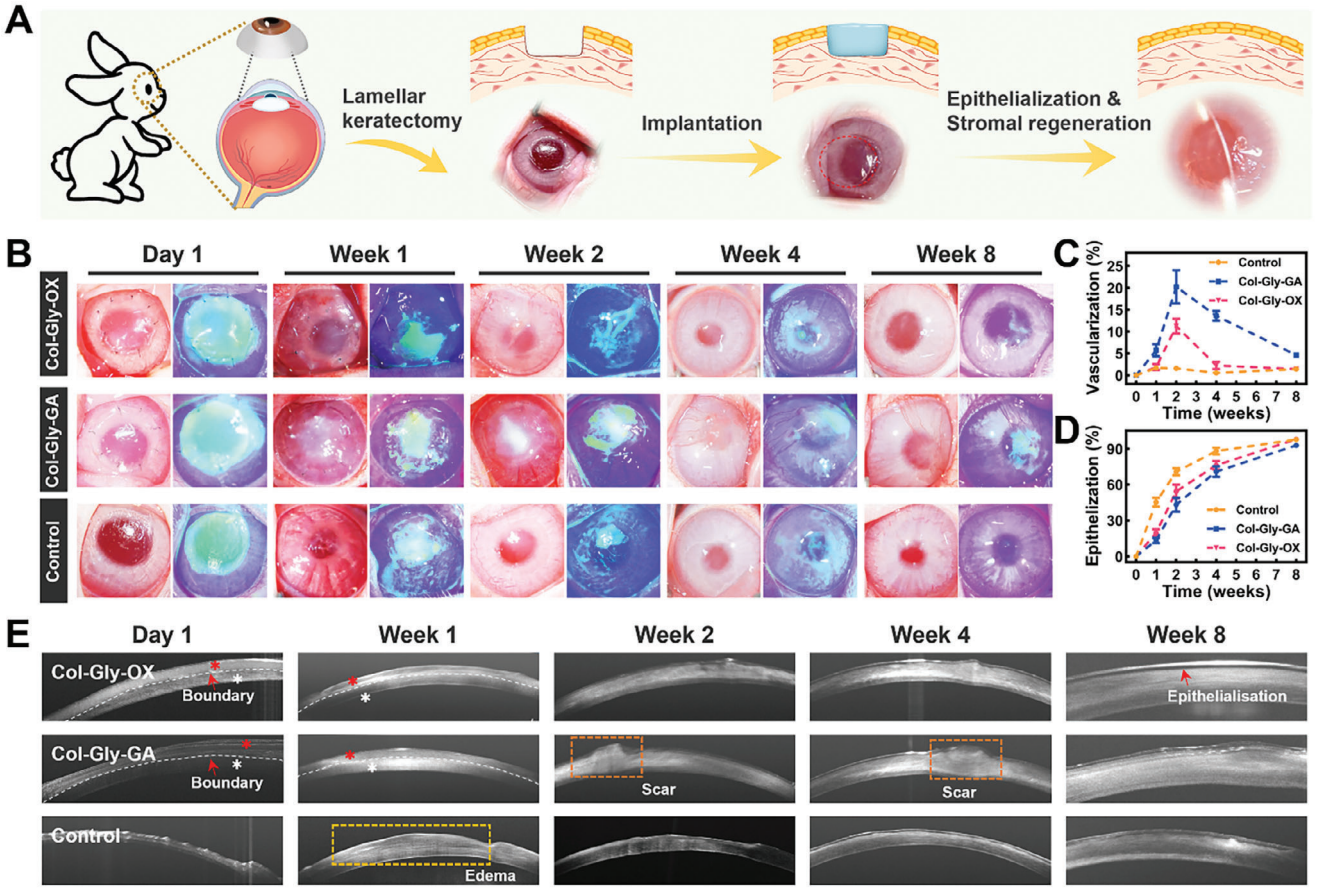

Figure 5. In vivo implantation A) Illustration of the corneal defect modelling and Col-Gly-OX implantation for re-epithelialization and stroma repair. B) Representative photographs of slit lamp and cobalt blue with fluorescein staining of the cornea after implantation. C) Quantitative statistics of vascular area ratio (n = 3) and D) The ratio of corneal epithelialization (n = 3). E) The images of rabbit corneas by anterior segment optical coherence tomography (AS-OCT) at different time points after implantation. Red asterisks denote the position of the implanted material, while white asterisks signify the location of the corneal stroma. The demarcation separating these entities is indicated by a white dashed line.

2.6. In Vivo Histological Evaluation of Artificial Corneal Substitute

Histological examinations were performed on the cryo-sectioned corneal tissues 8 weeks after surgery. H&E staining in **Figure 6A** showed that Col-Gly-OX integrated well with the underlying host stroma tissue, and no significant inflammatory cell infiltration or peripheral neovascularization was observed. However, significant inflammatory response and neovascularization exhibited in the Col-Gly-GA group, which may be due to its residual toxicity or fragility resulted mechanical mismatch. Statistics in Figure 6D,E confirmed that the epithelium and stroma thickness in the Col-Gly-OX group was closest to that of the native corneas, while much thinner in both the control and Col-Gly-GA group.

The immunofluorescence staining was further performed to evaluate the fibrosis and epithelialization (Figure 6B,C). The green fluorescence of α-SMA was hardly observed in the Col-Gly-OX group, similar to that of healthy cornea, indicating the inhibited myofibroblast formation and corneal scarring. However, positive staining of α-SMA was observed in the subepithelial location of the cornea in the Col-Gly-GA group, suggesting that keratocytes were activated and differentiated into SMA-positive myofibroblasts. It may be related to the poorer histocompatibility of the Col-Gly-GA group (Figure 6F). In addition, a tight junction protein ZO-1 in the epithelial monolayer was expressed in the Col-Gly-OX group, which almost equivalent to that of healthy cornea (Figure 6G), significantly higher than that in the Col-Gly-GA group. This result indicated that Col-Gly-OX acts as an ideal corneal alternative can enhance tissue integration, avoid overactivation of myofibroblasts, and support the regeneration of tight epithelial junctions.

3. Conclusion

We have demonstrated a green, simple and effective strategy for the development of transparent collagen matrix by treating thermo-assembled collagen hydrogels with glycerol. The glycerol treatment enabled collagen undergoing a multiscale structural transformation to achieve bottom-up ordered assembly and spacing rearrangement. Such a simple process causes a reasonable combination of fibril size and interfibrillar spacing to reconcile collagen thickness, transparency, and permeability. Hydroxylmethyl bicyclic oxazolidine crosslinking further created a full collagen-based artificial corneal substitute (Col-Gly-OX). It displayed an integration of multiple high-performance

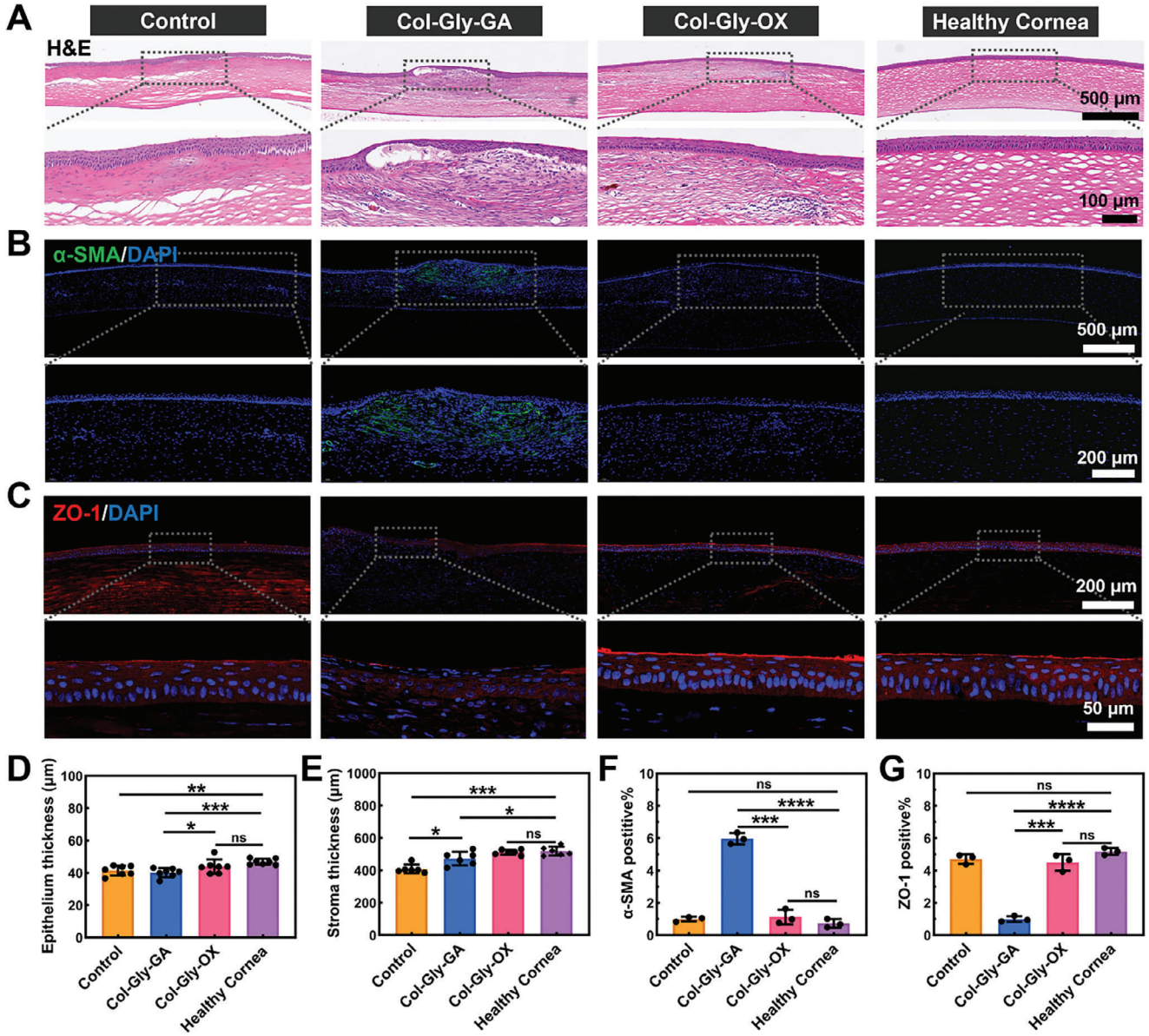

Figure 6. Histological analysis of the corneas after 8 weeks of Col-Gly-OX implantation. A) H&E, B) α-SMA, and C) ZO-1 immunofluorescence staining images. D) Quantification of epithelium thickness and E) stroma thickness according to the results from H&E staining. F) Quantitative α-SMA and G) ZO-1 expression from fluorescence staining images (n = 3). The values are mean ± SD. p-Values: $^{*}p < 0.05$, $^{**}p < 0.01$, $^{***}p < 0.001$ and $^{****}p < 0.0001$.

metrics, such as adequate thickness (up to centimeter level), excellent optical clarity (>90% light transmittance, <20% haze), permeability (93.69 ± 5.9 barrer), tensile and suture strength (1.6 MPa and 50gf), alongside long-term optical and structural stability. In vivo studies showed that Col-Gly-OX can effectively support epithelialization and stromal remodeling, and restore a transparent cornea within 8 weeks of corneal transplantation. Considering the optimal performance, convenient manufacturability and simple preservation, Col-Gly-OX therefore would be a potential artificial cornea with clinical application prospect, especially in wartime or other emergency situations.

4. Experimental Section

Materials: Type I collagen was obtained from Engineering Research Center in Biomaterials, Sichuan University. It was extracted from calf-skin through pepsin treatment and salt precipitation. Purification of the solubilized collagen was accomplished by sodium chloride fractionation and fibril assembly.[53] Acetic acid, glutaraldehyde, sodium hydroxide, trimethylaminomethane, paraformaldehyde, toluene, ethyl acetate and glycerin were obtained from Chengdu Kelon Chemical Co., Ltd. (China). Fluorescein diacetate (FDA), propidium iodide (PI), and methyl thiazolyl tetrazolium (MTT) were obtained from Sigma-Aldrich. Human corneal epithelial cells (HCECs) were obtained from Shanghai HonSun Biological Technology Co., Ltd. All reagents are used without further purification.

Preparation of Transparent Collagen Hydrogel: Briefly, collagen was dissolved in 0.5 M acetic acid solution and adjusted to pH = 7 by adding 5 M NaOH at 4 °C. Then, the hydrogel precursor solution was poured into cylindrical polystyrene molds (Φ 8 mm × 2 mm) and transferred to a 37 °C incubator for 30 min to obtain an opaque collagen hydrogel (Col). Transparent collagen hydrogels (Col-Gly) were obtained by immersing Col in various concentrations (20%, 40%, 60%, 80%, 100%) of glycerol solutions.

Synthesis of Hydroxylmethyl Bicyclic Oxazolidine: OX was synthesized by a modified procedure according to the literature.[45,46] Briefly, trimethylaminomethane (10.00 g, 82.6 mmol) and paraformaldehyde (5.70 g, 190.1 mmol) were dissolved in toluene (200 mL) in a 500 mL three-mouth flask and heated to reflux for 8 h. After the reaction, toluene was removed by rotary evaporation and the crude compound was recrystallized with ice ethyl acetate. The target product OX was obtained as a white solid. The chemical structure of OX was characterized by ^{1}H nuclear magnetic resonance (^{1}H NMR) spectroscopy (AV II-600 MHz, Bruker, 25 °C) by using D_2O as solvent.

Hydrogel Crosslinking: The prepared Col-Gly hydrogel was placed in a beaker containing 80% glycerol solution (in which the concentration of oxazolidine was 2%) with the aim of preventing the Col-Gly hydrogel from reassembling during crosslinking. After crosslinking for 5 min, the hydrogel was removed and placed in PBS solution. The solution was changed every 3 h for a total of 3 days to ensure the complete removal of glycerol and unreacted crosslinking agent. The final product was designated as Col-Gly-OX. A similar procedure was followed for the preparation of Col-Gly-GA, with GA replacing OX as the crosslinking agent.

Optical Characterization: The transmittance (%) of hydrogel films was measured by a UV–visible spectrophotometer (U-3900, Hitachi, Japan). Specifically, the hydrogel film was made into a circle with a diameter of 8 mm and a thickness of 400mm. After baseline calibration, the film was placed on a slide and placed on the light transmission hole of the instrument. The transmittance (%) was determined within the wavelength range of 380–800 nm, using a step size of 2 nm. In addition, the long-term transmittance of hydrogel films immersed in artificial tears for 0, 1, 2, 4, and 8 weeks was measured as described above. Haze spectra of the hydrogel film under normal incidence irradiation from 380 to 800 nm were monitored on the UV–vis-near-IR spectrometer (Lambda 950, PerkinElmer, America) with an integrating sphere. The general formula for calculating the haze value was given by Equation (2):

$$\text{Haze} = \frac{T_d}{T_t} \times 100\% = \left(\frac{T_4}{T_2} - \frac{T_3}{T_1}\right) \times 100\% \quad (2)$$

wherein, incident light sample (T_1), total transmittance (T_2), light scattering rate of the instrument itself (T_3) and sample diffusion rate (T_4) are obtained using an integrating sphere.

Microstructure Observation: The fibrillar structures of collagen hydrogels were taken on transmission electron microscopy (TEM, JEM-1400Flash, JEOL, Japan electronic), atom force microscope (AFM, Dimension Icon, Bruker, Germany), confocal laser microscopy (CLSM, LSM880, Carl Zeiss, Germany). Specifically, the collagen hydrogels were postfixed in 1% osmium tetroxide and embedded in Eponate 12 resin. After sectioning, these slices were stained with 1% phosphotungstic acid for 1–2 min, and finally observed using transmission electron microscopy. Statistics on fibril orientation and size in TEM images using Image J software. Notably, the fiber structure of the wet collagen hydrogels was observed using a reflection mode of a confocal laser scanning microscope. Moreover, the surface and cross-section morphology were also observed by scanning electron microscope (SEM, S-4800, Hitachi) at an acceleration voltage of 5.0 kV. Prior to this process, the hydrogel samples need to be frozen quickly with liquid nitrogen and then lyophilized using the freeze dryer (Advantage Plus EL-85, VirTis). The surface roughness of Col-Gly-OX film was measured by optical 3D surface profiler (SuperView W1, Chotest).

FTIR Analysis: The interaction between Col hydrogel and glycerol was characterized via a fourier transform infrared spectroscopy (FTIR; Nicolet 6700, Thermo Fisher, USA). Before the test, Col hydrogels treated with glycerol were rinsed with PBS to remove surface glycerol, and then lyophilized for 48h.

CD Analysis: Circular dichroism (CD) spectra (Chirascan plus, Applied photophysics) was used to measure the conformation of the collagen. The Col sample was prepared by dissolving Type I collagen in 0.5 mol L^{-1} acetic acid solution to achieve a concentration of 1 mg mL^{-1}. The Col-Gly sample was obtained by adding glycerol with different concentrations (0, 20, 40, 60, 80 and 100%) to the collagen solution. The samples were placed in a 1 mm path length quartz cuvette. Wavelength scanning was conducted from 185 to 260 nm at a scan speed of 50 nm min^{-1} and a temperature of 25 °C.

DSC Analysis: The changes in the melting temperature of hydrogels were measured using differential scanning calorimetry (DSC; DSC3+/500, METTLER TOLEDO, Switzerland). Under nitrogen protection, the hydrogels were cooled to −40 °C at a rate of 10 °C min^{-1}. Subsequently, the hydrogels were heated back to 20 °C at the same rate.

XRD Analysis: The crystalline structure of collagen hydrogels treated with different concentrations of glycerol was determined through X-ray diffraction (XRD; EMPYREAN, Panalytical, Netherlands). Before testing, these hydrogels were rinsed with PBS to remove surface glycerol, and then lyophilized for 48h.

Raman Spectroscopy Characterization: The Raman spectra of the hydrogel samples were collected by a DeepBlue200 confocal micro-Raman spectrometer (Southwest Spectro Technology co., Ltd). A single-crystal silicon standard was used for calibration. All spectra were obtained using a 532 nm laser through line scanning mode within the range of 100 to 4500 cm^{-1}.

2D SAXS Analysis: 2D Small-angle X-ray Scattering (2D SAXS) profiles of the hydrogel samples were collected with an X-ray detector of Pilatus 300K (Xeuss 2.0, Xenocs France). During 2D SAXS measurements, the distance between the sample and the detector was maintained at 88 mm. The software of Foxtrot was used to process the data.

Enzymatic Degradation Test: The prepared hydrogel samples were dried and weighed (W_0), and then immersed in PBS containing collagenase (150 U mL^{-1}) at 37 °C. At specific time points, the samples were removed from the liquid, dried, and reweighed (Wt). The degradation rate of the samples was obtained using the following Equation (3):

$$\text{Degradation ratio}\ (\%) = \frac{W_0 - W_t}{W_0} \times 100\% \quad (3)$$

Swelling Ratio Test: The prepared hydrogels were weighed and the initial weight was recorded as W_0. The hydrogel samples were then immersed in PBS. At specific time points, the hydrogels were retrieved, excess moisture was blotted off, and the wet weight was recorded as W_t. The swelling ratio was determined using Equation (4):

$$\text{Swelling ratio}\ (\%) = \frac{W_t - W_0}{W_t} \times 100\% \quad (4)$$

Saturated Water Content and Glycerol Content Test: The saturated water content of the hydrogels was calculated based on the weight change between the fully saturated and completely dry states. Specifically, the prepared hydrogel samples were freeze-dried and weighed, recorded as W_1. Then, the dried samples were immersed in PBS for 24 h to reach a fully saturated state, after which they were weighed again, recorded as W_2. The saturated water content of the samples was calculated using the following Equation (5):

$$\text{The saturated water content}\ (\%) = \frac{W_2 - W_1}{W_2} \times 100\% \quad (5)$$

The glycerin content is calculated by the following formula:

$$\text{The glycerin content}\ (\%) = \frac{W_h - W_w - W_d}{W_h} \times 100\% \quad (6)$$

wherein, total weight of collagen hydrogel (W_h), water weight of collagen hydrogel (W_w), dry weight of collagen hydrogel (W_d) are obtained by weighing.

Polarizing Microscope Observation: The optical images of the hydrogel were obtained by polarized optical microscopy under crossed polarizers with a λ plate (Axio Lab.A1, Zeiss). Briefly, Collagen hydrogels treated with different concentrations of glycerol were placed on a carrier stage to find the fiber structure at different focal levels by adjusting the focal lengths. In addition, a solution of glycerin and water in the ratio of 4:1 was used to treat the collagen films in the dry state, and the morphological changes of the films in the above liquid medium were observed under POM.

Mechanical Performance Test: Tensile testing was performed on the chemically cross-linked hydrogels, which were made into rectangular tensile test strips (5 mm in width and 25 mm in length). The tensile properties and suture strength of the chemically cross-linked hydrogels were studied by using a dynamic mechanical analysis (DMA, TA-Q800) tester. The tensile speed of the samples was 0.02mm $^{-1}$s for both tensile and suture tests, and the load versus displacement values and fracture strain values were also recorded. The tensile strength and elongation at break are calculated from the tensile stress-strain curve. In addition, mechanical stability under consecutive stress relaxation behavior was evaluated by rheometer (Anton Paar MCR302). The relaxation time was 120s and the strain values were 10%, 20%, 40%, 60% and 80%, separately.

Cell Proliferation Test: Human corneal epithelial cells (HCECs) were cultured in high-glucose DMEM (Hyclone) with 1% penicillin/streptomycin (Hyclone) and 10% fetal bovine serum (FBS, Every Green) at 37 °C with 5% CO_2. When HCECs were fully spread, they were trypsinized, collected, and subsequently seeded onto sterilized hydrogel samples. In 24-well plates, 2000 cells were seeded per well. For the control group, only cells were seeded without placing the hydrogel. Standard fluorescein diacetate–propidium iodide (FDA/PI) double staining and 3-(4,5-dimethylthiazol-2-yl)-2,5-diphenyltetrazolium bromide (MTT) assay were used to observe cell viability at 1 and 5 days. The stained cells were then imaged using a confocal laser scanning microscope (CLSM, Carl Zeiss-LSM880).

Cell Migration Test: To assess cellular migration using the scratch assay, HCECs were first seeded onto sterile hydrogel samples and allowed to grow until they formed a confluent monolayer. A straight scratch was then gently made on the surface of the monolayer using the tip of a 1 mL pipette. Images were captured using an inverted microscope (DMi8 S, Leica) at 0 and 36 h post-scratch to record the positions of cell migration. Cells were seeded only in a 24-well plate as a control. The scratch area was measured using ImageJ software, and the cell migration rate was calculated using the following Equation (6):

$$\text{migrationrate}\ (\%) = \frac{S_t}{S_0} \times 100\% \tag{7}$$

(S_0: initial scratch area, S_t: the scratch area at 36 h).

Animal Studies: All in vivo experiments were reviewed and approved by the Animal Care and Use Committee of Sichuan University (KS2023352). Male New Zealand white rabbits aged 10 to 12 weeks (Chengdu Dossy Experimental Animals Co., Ltd.) were selected for rabbit lamellar corneal surgery in this study. General anesthesia was induced in rabbits through intravenous injection of 2% pentobarbital sodium (30 mg kg^{-1}), and topical ocular anesthesia was achieved using 0.4% ophthalmic oxybuprocaine hydrochloride eye drops (2–4 drops per eye). A 7 mm trephine was employed to create a defeat at a depth of 250 µm in the central host cornea, and the lamellar cornea is then peeled off at the same depth with an ophthalmic scalpel. Custom-fabricated molds were employed to prepare Col-Gly-GA and Col-Gly-OX films with curvature, while meticulously controlling the thickness to ≈250 µm. The customized samples were sterilized through immersion in 75% alcohol and exposure to ultraviolet light. Then, Col-Gly-GA and Col-Gly-OX were filled in the defect site and secured with 10.0 nylon sutures, respectively. Moreover, the group with no material implanted into the corneal defect served as the control. The sutures are gently removed 10 days post-operation, following the stabilization of the epithelialization process in the cornea.

Slit-lamp and Anterior Segment Optical Coherence Tomography (AS-OCT) Evaluation: Weekly slit-lamp biomicroscopy (using SL-19, KOWA) was conducted to assess graft attachment, corneal clarity, and any pathological changes (including corneal scarring and neovascularization) in the experimental eyes. Corneal epithelial defects were evaluated using fluorescein staining under cobalt-blue illumination. Cross-sectional images of the cornea were captured weekly via AS-OCT to further examine the integration of the implants with the surrounding tissues under general anesthesia at 1, 2, 4, and 8 weeks postoperatively.

Histological Evaluation: The rabbits were humanely euthanized after 8 weeks. The excised eye tissues were fixed overnight in 4% paraformaldehyde. Following standard paraffin embedding and sectioning, the tissues underwent hematoxylin and eosin (H&E) staining. For immunofluorescence, antibodies against α-SMA, ZO-1, and DAPI were applied according to the protocol, and the sections were imaged using a fluorescence microscope.

Statistical Analysis: Unless otherwise noted, all error bars represented the mean ± standard deviation. All statistical analysis were carried out using one-way ANOVA test or *t*-test in Spass software or GraphPad Prism 9 software. Levels of significance was defined as $*p < 0.05$, $**p < 0.01$, $***p < 0.001$, and $****p < 0.0001$.

Supporting Information

Supporting Information is available from the Wiley Online Library or from the author.

Acknowledgements

This work is supported by the National Natural Science Foundation of China (Grant numbers: 52373150, 32361133548, 52303195 and 82403900), Natural Science Foundation of Sichuan Province (2023NSFSC0338, 2024NSFSC1014 and 2024NSFC1885), National Key Research and Development Program of China (2022YFC2402801), and Fundamental Research Funds for the Central Universities (2023SCUH0012).

Conflict of Interest

The authors declare no conflict of interest.

Author Contributions

Kai Wu: conceptualization, methodology, formal analysis, data curation, writing-original draft. Gaowei Li: methodology, software, investigation. Jiaze Gao: methodology, software, validation. Yuan Tian: methodology, investigation. Dan Wei: methodology, software. Chengheng Wu: formal analysis, methodology. Jie Ding: software, methodology. Jing Zhu: animal experiments, biological detection analysis. Hongrong Luo: investigation, methodology, formal analysis, writing-review & editing. Jing Sun: conceptualization, validation, formal analysis, funding acquisition, writing-review & editing. Seeram Ramakrishna: writing-review & editing; Hongsong Fan: conceptualization, methodology, resources, funding acquisition.

Data Availability Statement

The data that support the findings of this study are available from the corresponding author upon reasonable request.

Keywords

collagen, corneal regeneration, cornea substitute, fibril evolution, hydrogel

Received: August 27, 2024
Revised: December 4, 2024
Published online:

[1] A. Kumar, H. Yun, M. L. Funderburgh, Y. Du, *Prog. Retinal Eye Res.* **2022**, *87*, 101011.
[2] Y. Q. Soh, V. Kocaba, J. S. Weiss, U. V. Jurkunas, S. Kinoshita, A. J. Aldave, J. S. Mehta, *Nat. Rev. Dis Primers.* **2020**, *6*, 46.
[3] H. Zhou, S. Zhang, M. Lei, Y. Cai, H. Wang, J. Sun, J. Cui, C. Liu, X. Qu, *Bioact. Mater.* **2023**, *29*, 1.
[4] S. Meng, H. Hu, Y. Qiao, F. Wang, B. N. Zhang, D. Sun, L. Zhou, L. Zhao, L. Xie, H. Zhang, Q. Zhou, *ACS Nano* **2023**, *17*, 24055.
[5] P. Kumar, A. Pandit, D. I. Zeugolis, *Adv. Mater.* **2016**, *28*, 5381.
[6] K. M. Meek, C. Knupp, *Prog. Retinal Eye Res.* **2015**, *49*, 1.
[7] C. Raoux, A. Chessel, P. Mahou, G. Latour, M.-C. Schanne-Klein, *Light: Sci. Appl.* **2023**, *12*, 190.
[8] T. F. Gesteira, S. Verma, V. J. Coulson-Thomas, *Ocul. Surf.* **2023**, *29*, 521.
[9] M. Park, A. Richardson, N. Delic, K. Nguyen, J. Biazik, R. Zhang, L. Sprogyte, L. Nureen, J. Lees, A. Fajardo, U. Kunicki, S. L. Watson, J. Males, N. D. Girolamo, *Adv. Funct. Mater.* **2023**, *33*, 2304856.
[10] S. Majumdar, X. Wang, S. D. Sommerfeld, J. J. Chae, E. N. Athanasopoulou, L. S. Shores, X. Duan, L. M. Amzel, F. Stellacci, O. Schein, *Adv. Funct. Mater.* **2018**, *28*, 1804076.
[11] B. Kong, R. Liu, X. Hu, M. Li, X. Zhou, Y. Zhao, T. Kong, *Adv. Funct. Mater.* **2024**, *34*, 2310544.
[12] M. Lei, S. Zhang, H. Zhou, H. Wan, Y. Lu, S. Lin, J. Sun, X. Qu, C. Liu, *ACS Nano* **2022**, *16*, 10632.
[13] T. Almubrad, R. Mencucci, A. Smedowski, R. Samivel, S. Akhtar, *Saudi J. Biol. Sci.* **2021**, *28*, 7160.
[14] P. N. Lewis, C. Pinali, R. D. Young, K. M. Meek, C. Knupp, *Structure* **2010**, *18*, 239.
[15] G. H.-F. Yam, S. Pi, Y. Du, J. S. Mehta, *Prog. Retinal Eye Res.* **2023**, *96*, 101192.
[16] W. W. Kao, C. Y. Liu, *Glycoconjugate J.* **2002**, *19*, 275.
[17] M. P. Vena, L. S. van Hazendonk, W. van Zyl, R. Tuinier, H. Friedrich, *Small Methods* **2024**, *8*, 2301171.
[18] T. Suezawa, N. Sasaki, Y. Yukawa, N. Assan, Y. Uetake, K. Onuma, R. Kamada, D. Tomioka, H. Sakurai, R. Katayama, M. Inoue, M. Matsusaki, *Adv. Sci.* **2023**, *10*, 2302637.
[19] Y. W. Lim, J. Jin, B. S. Bae, *Adv. Mater.* **2020**, *32*, 1907143.
[20] H. Zhu, S. Parvinian, C. Preston, O. Vaaland, Z. Ruan, L. Hu, *Nanoscale* **2013**, *5*, 3787.
[21] T. Zhou, Z. Qiao, M. Yang, K. Wu, N. Xin, J. Xiao, X. Liu, C. Wu, D. Wei, J. Sun, *Biosens. Bioelectron.* **2023**, *231*, 115288.
[22] R. Mehrdad, J. Mahmoud, S. Namrata, X. Maria, T. Shideh, O. Raha, T. Muthukumar, M. Anthony, F. Per, L. Anton, *Nat. Biotechnol.* **2023**, *41*, 70.
[23] X. Sun, X. Yang, W. Song, L. Ren, *ACS Omega* **2020**, *5*, 674.
[24] J. Zhang, A. M. Sisley, A. J. Anderson, A. J. Taberner, C. Mcghee, D. V. Patel, *Tissue Eng., Part C* **2015**, *22*, 165.
[25] C. Salameh, F. Salviat, E. Bessot, M. Lama, N. Nassif, *Proc. Natl. Acad. Sci* **2020**, *117*, 11947.
[26] H. Tao, B. Lin, *Colloid Polym. Sci.* **2017**, *295*, 205.
[27] J. Pan, W. Zhang, J. Zhu, J. Tan, Y. Huang, K. Mo, Y. Tong, Z. Xie, Y. Ke, H. Zheng, H. Ouyang, X. Shi, L. Gao, *Adv. Mater.* **2023**, *35*, 2207750.
[28] G. Young, R. Bowers, B. Hall, M. Port, *CLAO J* **1997**, *23*, 249.
[29] N. P. D. Tran, M. C. Yang, *Polymers* **2020**, *12*, 1128.
[30] K. Liu, L. Li, J. Chen, Y. Li, W. Wen, L. Lu, L. Li, H. Li, M. Liu, C. Zhou, B. Luo, *ACS Nano* **2022**, *16*, 21020.
[31] Y. Niu, J. Chen, Z. Geng, W. Wu, H. Cai, C. Liu, P. Cao, Y. Zhang, Y. Liu, A. Qiao, T. Du, *Mater. Des.* **2024**, *239*, 112830.
[32] M. Winkler, G. Shoa, Y. Xie, S. J. Petsche, P. M. Pinsky, T. Juhasz, D. J. Brown, J. V. Jester, *Ophthalmol. Visual Sci.* **2013**, *54*, 7293.
[33] Y. Wang, L. Xu, J. Zhao, J. Liang, Z. Zhang, Q. Li, J. Zhang, P. Wan, Z. Wu, *Biomaterials* **2022**, *289*, 121745.
[34] M. Madeleine, G. Guille, G. Mosser Emmanuel, *Colloid Interface Sci.* **2008**, *13*, 303.
[35] C. Knupp, P. N. Lewis, C. Pinali, R. D. Young, K. M. Meek, A. J. Quantock, *Invest. Ophthalmol. Visual Sci.* **2009**, *50*, 4532.
[36] J. Regini, G. Elliott, S. Hodson, *J. Mol. Biol.* **2004**, *336*, 179.
[37] G. Elliott, S. Hodson, *Rep. Prog. Phys.* **1998**, *61*,1325.
[38] K. M. Meek, S. Dennis, S. Khan, *Biophys. J.* **2003**, *85*, 2205.
[39] N. Renier, Z. Wu, D. J. Simon, J. Yang, P. Ariel, M. Tessier-Lavigne, *Cell* **2014**, *159*, 896.
[40] A. Ertürk, K. Becker, N. Jährling, C. P. Mauch, C. D. Hojer, J. G. Egen, F. Hellal, F. Bradke, M. Sheng, H. Dodt, *Nat. Protoc.* **2012**, *7*, 1983.
[41] C. Tang, Y. Xu, K. Zhou, Y. Xie, Y. Ma, C. Li, F. Xu, H. Zhou, B. Xu, *Food Res. Int.* **2023**, *171*, 112985.
[42] F. Peng, X. Zhang, Y. Wang, R. Zhao, Z. Cao, S. Chen, Y. Ruan, J. Wu, T. Song, Z. Qiu, *Collagen Leather* **2023**, *5*, 5.
[43] R. Rai, R. Khazeber, K. M. Sureshan, *Angew. Chem., Int. Ed.* **2023**, *62*, e202315742.
[44] M. Matsusaki, R. Amekawa, M. Matsumoto, Y. Tanaka, A. Kubota, K. Nishida, M. Akashi, *Adv. Mater.* **2011**, *23*, 2957.
[45] T. Yu, X. Chen, W. Zhuang, Y. Tian, Y. Wang, *Chem. Eng. J.* **2021**, *414*, 128900.
[46] T. Yu, C. Zheng, X. Chen, H. Pu, G. Li, Q. Jiang, Y. Wang, Y. Guo, *Acta Biomater.* **2023**, *296*, 122070.
[47] K. Adamiak, A. Sionkowska, *Int. J. Biol. Macromol.* **2020**, *161*, 550.
[48] H. Pu, C. Wang, T. Yu, X. Chen, G. Li, D. Zhu, X. Pan, Y. Wang, *Int. J. Biol. Macromol.* **2024**, *266*, 130715.
[49] M. Lombardo, G. Lombardo, G. Carbone, M. P. Santo, R. Barberi, S. Serrao, *Invest. Ophthalmol. Visual Sci.* **2012**, *53*, 1050.
[50] Y. Hao, J. Zhou, J. Tan, F. Xiang, Z. Qin, J. Yao, G. Li, M. Yang, L. Zeng, W. Zeng, C. Zhu, *Bioact. Mater.* **2023**, *29*, 265.
[51] M. Ahearne, J. Fernández-Pérez, S. Masterton, P. W. Madden, P. Bhattacharjee, *Adv. Funct. Mater.* **2020**, 30.
[52] J. Hooton, M. Kyeong, H. Kim, S. I. MD, N. Lentz, K. Hicks, K. Jones, S. I. McCoy, *Cornea* **2019**, *38*, 1023.
[53] L. Zheng, H. S. Fan, J. Sun, X. N. Chen, G. Wang, L. Zhang, Y. J. Fan, X. D. Zhang, *J. Biomed. Mater. Res., Part A.* **2008**, *10*, 783.